

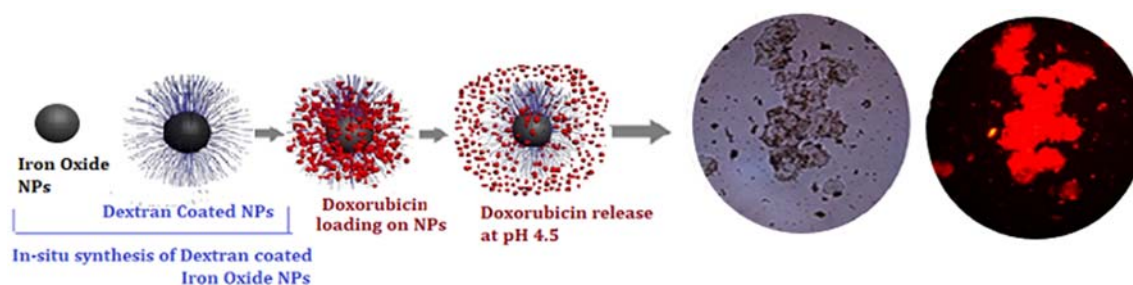
Doxorubicin-loaded magnetic nanoparticles downregulate expression of anti-apoptotic genes in resistant breast cancer cells

Serap Yalcin^{1*}, Pelin Mutlu², Gözde Unsoy³, Rouhollah Khodadust³, Ufuk Gunduz³

¹Department of Molecular Biology and Genetics, Kirsehir Ahi Evran University, 40100, Kirsehir, Turkey ²Central Laboratory, Molecular Biology and Biotechnology R&D Center, ³Department of Biological Sciences, Middle East Technical University, 06800, Ankara, Turkey

Submitted on: 07-Mar-2020 Accepted and Published on: 22-June-2020

ABSTRACT



In this research, the surface of magnetic nanoparticles (IO-NPs) was coated with dextran polymer (Dex-IO-NPs) in which dextran provides both cavities for drug loading and drug stability. Dex-IO-NPs were synthesized by co-precipitation of iron salts with ammonium hydroxide in the presence of dextran solution. Dex-IO-NPs were then characterized by FTIR, TGA, SEM, and VSM analyses. Doxorubicin was loaded on Dex-IO-NPs (Dox-Dex-IO-NPs) and applied to breast cancer (MCF-7) and Doxorubicin resistant (MCF-7/1000nM-Dox) breast cancer cell lines. Dex-IO-NPs were highly internalized and localized within the cells. Importantly, the half-maximal inhibitory concentrations (IC₅₀) of Dox-Dex-IO-NPs were 0.8 μ M and 25 μ M in MCF-7 and MCF-7/1000nMDox cells respectively, which were 2 and 7 times more effective in cell death with respect to free Doxorubicin. The release of the anti-cancer agents from Dox-Dex-IO-NPs occurs with the natural degradation of Dextran and allows nuclear uptake of Doxorubicin, which results in an increase in the efficacy of Doxorubicin. The anti-apoptotic genes were downregulated in Dox-Dex-IO-NPs treated cells as compared to free Doxorubicin treated cells, revealing the higher cytotoxicity and apoptotic potential of Dox-Dex-IO-NPs. These results imply that Dex-IO-NPs particles have the potential to be an efficient tool for drug delivery in breast cancer therapy.

Keywords: Dextran; iron oxide nanoparticles; drug resistant breast cancer; targeted drug delivery; apoptosis; gene expression

INTRODUCTION

The iron oxide-based nanoparticles (IO-NPs) have been investigated for diverse biomedical applications so far. Generally, IO-NPs are engineered to be used in magnetic cell separation, MR imaging as magnetic contrast agents, hyperthermia for thermal ablation of tumors, and targeted drug delivery as magnetic vectors

that can be directed towards tumor tissue.^{1,2}

The iron oxide-based nanoparticles (Fe₃O₄, core ranging between 10 nm and 100 nm diameter) are potent targeted delivery tools for biomedical applications.³ Anti-cancer agents loaded onto the nanoparticles are delivered to the target tissue by an external magnetic field. Nanoparticles are expected to stay in circulation after the injection. Furthermore, they pass through from capillary systems of organs and tissues to avoid embolism and thrombosis.⁴⁻⁶

Survivin (BIRC5) leads to negative regulation of apoptosis via inhibiting caspase activation. BIRC5 is overexpressed in most tumors and the disruption of Survivin pathways increases apoptosis and decreases tumor growth.⁷ The molecular mechanisms of BIRC5 regulation are still not clear, but studies

*Corresponding Author: Dr. Serap Yalcin, PhD, Department of Molecular Biology and Genetics, Kirsehir Ahi Evran University, 40100, Kirsehir, Turkey,

Email: syalcin@ahievran.edu.tr

Tel: +903862804543, Fax: +903862804525 :

Cite as: *J. Mat. NanoSci.*, 2020, 7(1), 29-35.

URN:NBN:sciencein.jmns.2020v7.126

©The ScienceIn ISSN 2394-0867 <http://thesciencein.org/jmns>

Journal of Materials NanoScience

demonstrated that survivin is associated with p53 protein.⁸ Up-regulation of Survivin could be regarded as an indication of Doxorubicin resistance.⁹ Bcl-2, apoptosis regulator, suppresses and regulates apoptosis by controlling the mitochondrial membrane permeability.¹⁰ Caspases are a family of aspartic acid-specific proteases and are crucial mediators of apoptosis.¹¹ Activation of caspases induces apoptosis and characterizes morphological cellular changes.¹²

The expression of Noxa (PAMP1) and Puma is p53 dependent in response to apoptotic stimuli.¹³ The p53 is a crucial protein in the regulation of the cell cycle and apoptosis.¹⁴

In this study, Dox-Dex-IO-NPs were designed and synthesized in order to be used in tumor-targeted drug delivery. In addition, we describe a new strategy to expression levels of apoptotic genes, using the drug-nanoparticle system. Dex-IO-NPs were produced by the *in situ* co-precipitation method, providing efficient, mild, and simple one-pot synthesis. Nanoparticles were characterized by FTIR, TGA, SEM, and VSM analyses. Doxorubicin was loaded into the biodegradable dextran layer of Dex-IO-NPs through non-covalent electrostatic interactions (Dox-Dex-IO-NPs). The stability, drug release, cytotoxicity, and efficacy of Dox-Dex-IO-NPs were analyzed on original and doxorubicin-resistant MCF-7 breast cancer cell lines. Besides the expression profiles of some pro-apoptotic and anti-apoptotic genes including Survivin, Bcl-2, Noxa, p53 in MCF-7, and MCF-7/1000nM Dox cell lines were studied under the treatment of Dox-Dex-IO-NPs and free Doxorubicin.

MATERIAL AND METHODS

Iron (II) chloride tetrahydrate ($\text{FeCl}_2 \cdot 4\text{H}_2\text{O}$), iron (III) chloride hexahydrate ($\text{FeCl}_3 \cdot 6\text{H}_2\text{O}$), Dextran polymer, ammonium hydroxide (NH_4OH), phosphate buffered saline (PBS), RPMI-1640, Doxorubicin and XTT kit were obtained from Sigma-Aldrich (USA). FTIR spectra were obtained by Thermo Scientific Nicolet 6700 FTIR spectrometer. XRD (X-Ray Diffraction Spectroscopy) and Zeta-Potential measurements were carried out at METU.

In Situ Synthesis of Dex-IO-NPs

Dex-IO-NPs were *in situ* synthesized by the co-precipitation of iron salts in the presence of dextran molecules. The iron salts were dissolved in water. Then, the ammonia (32 % NH_4OH , 25 ml) and dextran (5% (w/v) in water) solutions were added to the mixture very slowly under the nitrogen (N_2) gas flow by vigorous stirring at 2500 rpm. *Dex-IO-NPs* (Figure. 1 B) were extensively washed with water (deionized) and separated by magnetic decantation.

Biochemical Characterization of Dex-IO-NPs

Synthesized Dex-IO-NPs were characterized by FTIR, TGA, VSM, and SEM analyses. The chemical coactions were defined by using the Fourier Transform Infrared spectroscopy (FTIR). The morphology, size range and structural properties of Dex-IO-NPs were observed through SEM image analyses. The quantitative information about the volatile compounds of the nanoparticles has been provided by Thermogravimetric analysis (TGA). TGA was performed with 3–5 mg sample, between 30 °C to 850 °C temperatures in argon atmosphere. Magnetic properties of IO-NPs were determined by Vibrating Sample Magnetometer (VSM) analyses.

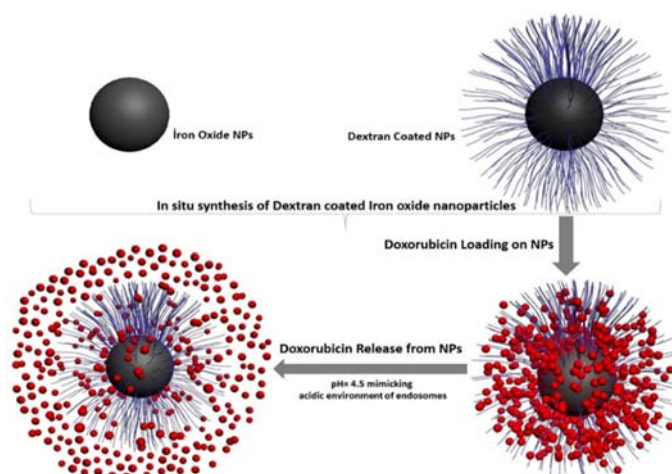


Figure 1. Schematic view of Doxorubicin loading and release from synthesized dextran coated iron oxide nanoparticles

Doxorubicin Loading on Dex-IO-NPs

The different molarities mix of Doxorubicin were stirred by Dex-IO-NPs (2.5 mg/ml) in methanol solution (100%). After the incubation period, Dox-Dex-IO-NPs were separated by magnetic decantation, and drug loading efficiency was quantified by measuring the amount of drug remained in supernatant (Equation 1) with a UV spectrophotometer (Multiskan GO, Thermo Scientific) at 482 nm. Amount of the free Doxorubicin in supernatant was calculated by using standard curve.

Equation

$$\text{Drug entrapment (\%, w/w)} = \frac{(\text{Mass of the total drug} - \text{Mass of free drug}) \times 100}{\text{Mass of total drug}}$$

Release of Doxorubicin from Dox-Dex-IO-NPs

The release of Doxorubicin from Dox-Dex-IO-NPs was analyzed for different pH values (in acetate (pH 4.5) and PBS (pH 7.2) buffers) at 37 °C. The Doxorubicin release from Dextran-MNPs were analyzed in acetate buffer at two different pH values (pH 4.5 and pH 7.2), which mimics endosomal and lysosomal conditions. Amount of the Doxorubicin released from Dox-Dex-IO-NPs was determined by measuring the absorbance of supernatant with UV-vis spectrophotometer (482 nm) at different time intervals.

Cellular internalization of Dox-Dex-IO-NPs

In order to visualize the cellular internalization of nanoparticles; Dox-Dex-IO-NPs and breast cancer cells were incubated for 4 hours. Then the images of the cells were taken by fluorescence microscopy (Figure 6).

Cytotoxicity of free Doxorubicin and Dox-Dex-IO-NPs

Cytotoxicity of free Doxorubicin and Dox-Dex-IO-NPs on MCF-7 and MCF-7/1000nM Dox cells were determined by XTT Cell Proliferation Assay. According to the instructions of manufacturer, XTT reagent was added after the cells were exposed to different concentrations of Doxorubicin and Dox-Dex-IO-NPs, for 72 hours. The cell viability of control groups was considered hundred percent. Amount of soluble product formazan dye was measured at 496 nm by microplate reader (Multiskan GO, Thermo Scientific) and IC_{50} values were calculated.

Expression levels of apoptosis-related genes

MCF-7 and MCF-7/1000nM Dox cells were seeded in 6-well plates. After overnight incubation, the cells were treated with free Doxorubicin and Dox-Dex-IO-NPs at the concentrations equal to their IC₅₀ values. RNA isolation was performed by using TriPure RNA isolation reagent (Roche Life Sciences, USA). RNA quality and quantity were checked by spectrophotometric analysis (Nanodrop, Thermo Scientific, USA) and performing agarose gel electrophoresis. For the samples having low A260/A230 ratios, salt precipitation was performed by sodium acetate. cDNA synthesis was done by using random hexamer primers and qPCR was performed. Fold changes of gene expression values are given relative to untreated MCF/7 controls.

RESULTS

Biochemical Characterization of Dex-IO-NPs

FTIR Analysis of Dox-Dex-IO-NPs and Dex-IO-NPs

FTIR spectra of Dox-Dex-IO-NPs, Dex-IO-NPs and Doxorubicin are shown in Figure 2. The spectra of Dox-Dex-IO-NPs (Figure.2 a) and Dex-IO-NPs(Figure.2 b) shows peaks at 3372 cm⁻¹, 1363 cm⁻¹, 1126 cm⁻¹ and 916 cm⁻¹. These peaks are almost the same as the main characteristic absorption peaks of the dextran at 3700–3200 cm⁻¹ (H-OH), 1138 and 1020 cm⁻¹ (O-H). The Fe-O vibrational stretch was observed in both Dox-Dex-IO-NPs (Figure.3 a) and Dex-IO-NPs at 596 cm⁻¹ (Figure.2 b). Absorption peaks at 2932 (C-H), 1730 (C=O), 1618 and 1577 (N-H), 1414 (C-C) and 1071 (C-O) cm⁻¹, belonging to Doxorubicin was also seen in the spectrum of Dox-Dex-IO-NPs (Figure.2 a). These results confirm that the presence of Doxorubicin on dextran coated IO-NPs.

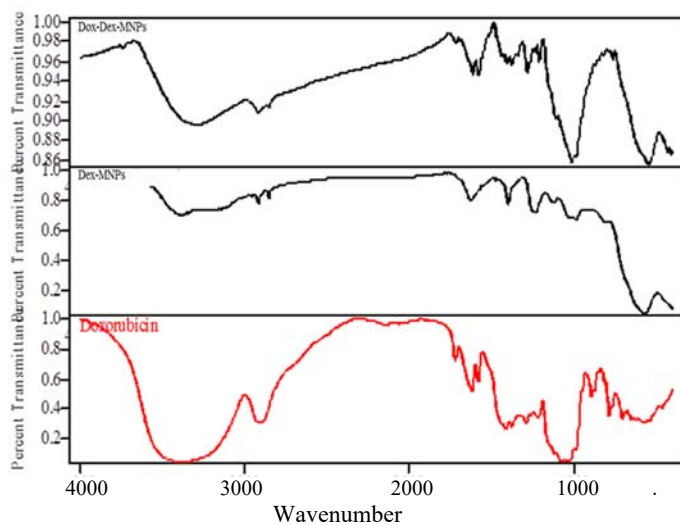


Figure 2. FTIR spectra of Dox-Dex-IO-NPs(a), Dex-IO-NPs(b) and Doxorubicin (c).

TGA Analysis of Dex-IO-NPs

TGA was used to investigate the amount of the dextran coat on the surface of IO-NPs over the temperature range from 30 to 850 °C (Figure 3). The weight loss of MNP core is about 3%. The loss of residual water can cause 3 % weight loss for MNP core in the sample. The weight loss of Dex-IO-NPs is about 10 %, so, the average amount of dextran on Dex-IO-NPs was found to be 7 % by weight.

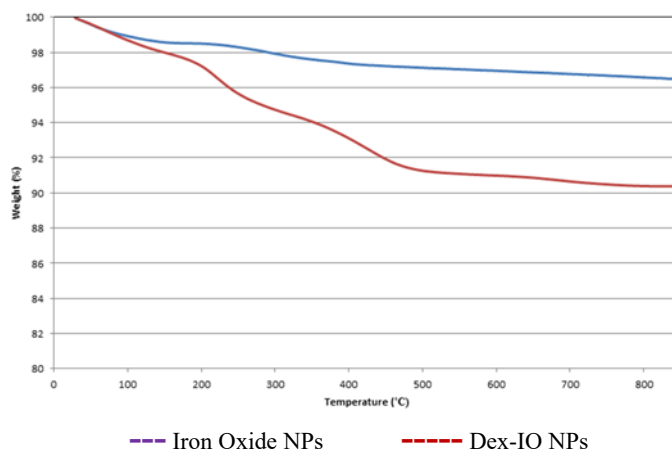


Figure 3. TGA plots of bare IO-NPs and Dex-IO-NPs

SEM Analyses of Dex-IO-NPs

The size, shape and surface morphology of prepared Dex-IO-NPs were observed through SEM images. Diameter of Dex-IO-NPs estimated from 10-15 nm from SEM image (Figure 4). Most of the nanoparticles were fairly at spherical shape however, surface of the particles showed a porous characteristic.

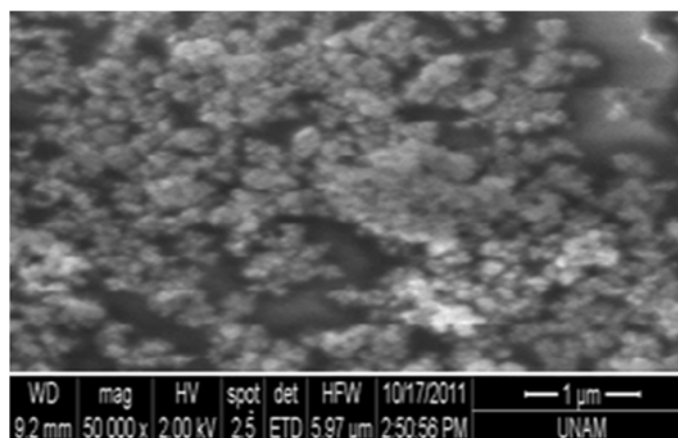


Figure 4. SEM image of Dex-IO-NPs

VSM Analysis of Dex-IO-NPs

Magnetic properties of Dex-IO-NPs were determined by magnetic hysteresis curve (VSM analysis) (Figure 5). The applied magnetic field was changed and magnetization properties of

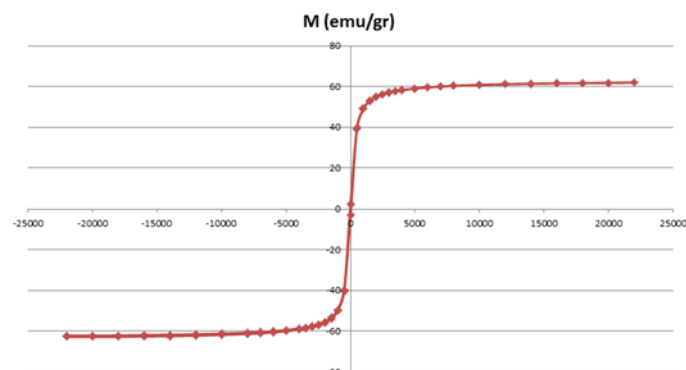


Figure.5 Hysteresis curve of Dex-IO-NPs

synthesized Dex-IO-NPs were measured at 37°C. The saturated magnetization (M_s) value was found as 62 emu/g. No remanence and coercivity was observed in the hysteresis curves pointing out the superparamagnetic property of Dextran coated iron oxide core nanoparticles.

Doxorubicin Loading on Dex-IO-NPs

Doxorubicin loading was achieved as 415, 530, 715 and 893 μM with different initial drug concentrations of 442, 552, 737, 921 μM , respectively (Figure 6). The highest loading efficiency was determined as 97% (893 μM) with the highest Doxorubicin concentration (500 $\mu\text{g/ml}$).

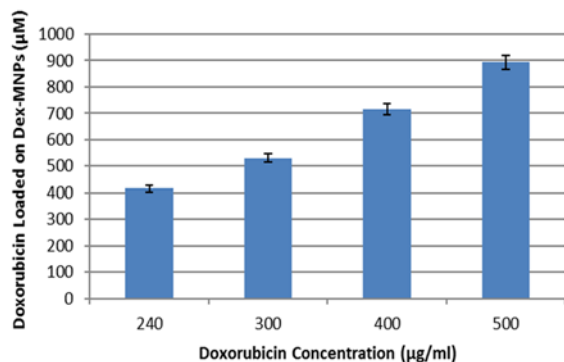


Figure 6. Doxorubicin loaded on Dex-IO-NPs at different drug concentrations. The data are represented as the mean \pm SEM ($n=3$).

Release of Doxorubicin from Dox-Dex-IO-NPs

The release of Doxorubicin from Dox-Dex-IO-NPs was studied at pH 4.5 and pH 7.2 for 5 days (Figure 7). The maximum amount of Doxorubicin released was 20 % and 66 % at pH 7.2 and pH 4.5, respectively. The release reached saturation in 15 h at both pH values. It is observed that Dox-Dex-IO-NPs exhibited a slow, steady and pH controlled release of the drug over a 60 h period.

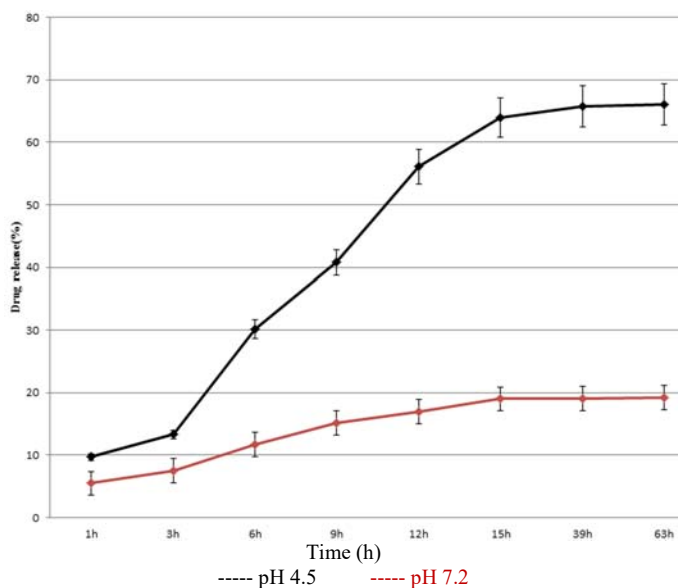


Figure 7. Drug release plot of Dox-Dex-IO-NPs at acidic (pH 4.5) and neutral (pH 7.2) pHs

Cellular internalization of Dox-Dex-IO-NPs

Fluorescence microscopy indicated high amounts of cellular internalization and accumulation of free doxorubicin and Dox-Dex-IO-NPs both in the cytoplasm and nucleus of MCF-7 and MCF-7/1000nM Dox cells (Figure 8 and 9).



Figure 8. Fluorescent images of free Doxorubicin internalized MCF-7 cells at 40x resolution. (DAPI stain labelled nuclei of the cells)

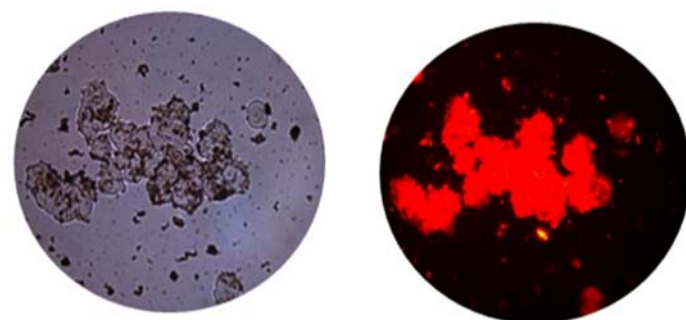


Figure 9. Fluorescent images of Dox-Dex-IO-NPs internalized MCF-7 cells at 40x resolution.

Cytotoxicity of Dox-Dex-IO-NPs

Dex-IO-NPs showed very low cytotoxicity to MCF-7 and MCF-7/1000nM Dox cells by 80% of cell viability at the highest nanoparticle concentration (750 $\mu\text{g/ml}$). Dox-Dex-IO-NPs showed high potency cytotoxicity at extremely low concentrations by showing IC_{50} of 0.8 μM and 25 μM on MCF-7 and MCF-7/1000nM Dox cells, respectively (Figure 10).

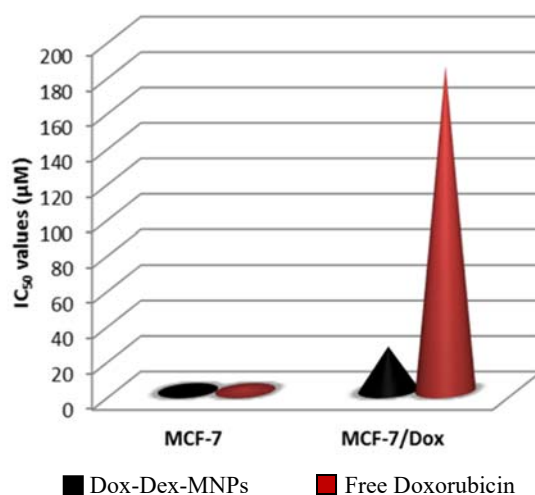


Figure 10. IC_{50} values of Dox-Dex-IO-NPs and free Doxorubicin on MCF-7 and MCF-7/1000nM Dox cells.

Expression levels of genes related to cell survival and apoptosis

Expression levels of different genes that are related to cell survival and apoptosis were investigated by qRT-PCR (Figure 11).

According to the q-PCR results, survivin gene expression was 3-fold upregulated in untreated MCF-7/1000nM Dox resistance cells as compared to untreated MCF-7 cells. However, survivin gene was downregulated due to the application of free Doxorubicin and Dox-Dex-IO-NPs in MCF-7/1000nM Dox cells. The Bcl-2 gene was approximately 5 fold downregulated in response to Dox-Dex-IO-NPs with respect to the application of free Doxorubicin on MCF-7/1000nM Dox cell lines. That can be concluded as, Dox-Dex-IO-NPs trigger apoptosis more than free Doxorubicin. Whereas, expressions levels of pro-apoptotic Noxa, caspase 3 and p53 genes did not change significantly in the treated and untreated MCF-7/1000nM Dox cell lines.

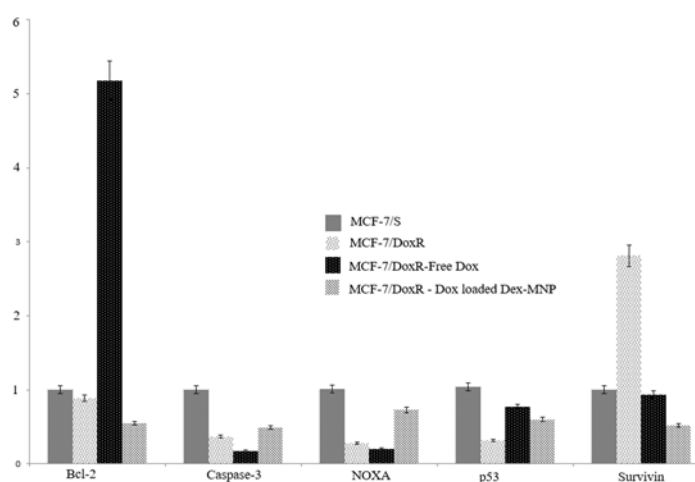


Figure 11. The fold change graph of gene expression levels on Dox-Dex-IO-NPs and free Doxorubicin treated MCF-7 and MCF-7/1000nM Dox cells.

DISCUSSION

Recently, various anticancer drugs have been conjugated/loaded with magnetic nanoparticles to enhance tumor targeting and to overcome drug resistance.^{15–17} Various strategies have been developed in order to enhance the efficacy and reduce the side effects of anti-cancer drugs.¹⁸ Targeted delivery of anti-cancer agent loaded onto the magnetic nanoparticles is a promising alternative to conventional chemotherapy.¹⁹ The core-shell structured polymeric magnetic nanoparticles have the advantages of good dispersion, high stability, providing functional groups, and the capacity to load more drugs into the polymer shell. The magnetic core inside the polymeric nanoparticles can be used for magnetic manipulation and imaging-based tracking of nanocarriers. The use of magnetic nanoparticles for the delivery of chemotherapeutic agents should provide not only drug delivery but also protection of the loaded drug. In addition, IO-NPs are promising nanocarrier for the targeting of cancer cells under the magnetic field.^{20–22} We have previously loaded Doxorubicin on chitosan (Cs-MNPs), dendrimer (Dc-MNPs) and

polyhydroxybutyrate (PHB-MNPs) coated magnetic nanoparticles at loading ratios of; 486 $\mu\text{g/ml}$, 384 $\mu\text{g/ml}$, 348 $\mu\text{g/ml}$, respectively.^{23–25}

Biocompatible and biodegradable dextran is preferably coated on IO-NPs to provide a drug conjugation shell. Dextran has been commonly analyzed in biomedical research. Due to the huge number of hydroxyl groups, it can be easily conjugated with anticancer agents by direct conjugation or incorporation of a linker molecule. The use of physical interactions such as electrostatic and hydrophilic/hydrophobic interactions is useful for the coupling of drug molecules on the polymeric surface of IO-NPs. Dextran, being a biodegradable polymer inside the cells, the loaded drug can be easily released.²⁶ In this study, dextran coated magnetic nanoparticles were firstly synthesized with a simple and efficient method. The synthesized Dex-IO-NPs were characterized by FTIR, TGA, SEM and VSM analyses. The peaks observed in FTIR verified the dextran coat on iron oxide nanoparticles. TGA revealed that the amount of dextran coat on Dex-IO-NPs was 7 % by weight. The particle size of Dex-IO-NPs was ranging between 10 - 15 nm. The morphology of Dex-IO-NPs was observed fairly smooth and spherical on SEM images. The saturated magnetization (Ms) value of nanoparticles was measured as 62 emu/g with no remanence and coercivity indicating the superparamagnetic property of Dextran coated iron oxide core nanoparticles.

Doxorubicin intercalates with DNA and inhibition of topoisomerase II occurs inside the nucleus to block DNA replication. Therefore, nuclear transport of IO-NPs through the nuclear pore complex is important.²⁷ Generally, scientists have demonstrated that intracellular localization of nanoparticles showed collection mostly in the cytoplasm.²⁸ In fact, nuclear localization of nanoparticles is complicated since the nuclear pores have a specific diameter of 30–40 nm and the diffusion rate through such small pore size depends on size, shape and surface chemistry of nanoparticles.

The highest loading efficiency of Doxorubicin was obtained at 97% (500 $\mu\text{g/ml}$). Polymer type and concentration, amount of the drug, shaker rate and shaking time play important roles in controlling the drug loading efficiency and achieving drug release at the target site. The interactions between Doxorubicin and nanoparticles directly influence the loading and release behavior of drugs *in vitro*.¹⁶ Magnetic nanoparticles coated with dextran, which have negative charged functional groups can couple with ionized Doxorubicin via electrostatic interactions.²⁹ Here we suppose that drug loading was achieved into the dextran coat on IO-NPs via electrostatic interactions of ionized Doxorubicin with the negatively charged hydroxyl groups exposed on the polymer. Instead of the weak interaction ways, including the hydrogen-bonding from -OH of dextran with the -OH and -NH groups in Doxorubicin, electrostatic interactions are constructed between the negative charges of Dex-IO-NPs and positive charges of Doxorubicin. In addition to this, physical adsorption of Doxorubicin onto the Dex-IO-NPs can also take place.

The drug release generally occurs by two mechanisms; the diffusion of drug molecules and degradation of the polymer matrix. So, every single variable that affects the polymer nature can change the drug release behavior. For instance, it was

represented that high polymer concentration effectively prevents the release of drug by forming thick polymer walls.³⁰ Zhang and Misra³¹ reported a thermosensitive smart polymer, dextran-g-poly (NIPAAm-co-DMAAm), can regulate drug release in response to temperature changes by swelling and deswelling in the vicinity of lower critical solution temperature (LCST) $\sim 40^{\circ}\text{C}$.

In this study, we have shown that Dox-Dex-IO-NPs effectively release the Doxorubicin in a pH-controlled manner. In neutral pH (pH 7.2), only 20 % of loaded drug was released from Dox-Dex-IO-NPs over a 60 h period. However, 66 % of the loaded Doxorubicin was released from Dox-Dex-IO-NPs at pH 4.5. This acidic range of pH, can be observed in the endosomes and tumor microenvironment. Doxorubicin release reached a saturation at 15 h and continued with a slow, steady state release for 63 hours.

Free Doxorubicin can pass through the cell membrane by diffusion which is driven by a concentration gradient. Due to its hydrophobic anthracycline backbone, cellular membrane is highly permeable to Doxorubicin. Therefore, free Doxorubicin passes through the cell membrane and part of it enters into the nuclei where it inhibits DNA replication.^{32,33}

Although, the easy passage of free Doxorubicin through the cell membrane, its hydrophobic structure is a disadvantage for the solubility in aqueous media. Another disadvantage of Doxorubicin application is its harsh cardiotoxic side effects. The development of drug resistance mechanisms is the other reason which restricts free Doxorubicin application in cancer chemotherapy.³⁴ On the other hand, Dox-Dex-IO-NPs are taken up into the cells by endocytosis which bypasses the drug resistance mechanisms. Doxorubicin is released from Dex-IO-NPs in a controlled manner inside the acidic endosomes, and diffused into the cytosol before it finally enters the cell nuclei.³⁵ It was observed that Doxorubicin was present both in cytoplasm and nuclei without any preference. To achieve high cytotoxicity, Doxorubicin should be delivered into nucleus to intercalate with DNA double helix. It is hypothesized that the nuclear delivery of nanoparticles larger than the size of nuclear pore (30-40 nm) is not possible. The synthesized Dex-IO-NPs may easily pass through the nuclear pores due to their small size (10-15 nm) or internalized by the cells and Doxorubicin was released through spontaneous degradation of dextran, allowing free diffusion of Doxorubicin from cytoplasm into nucleus.

According to *in vitro* cytotoxicity analysis, Doxorubicin efficacy was increased when applied as loaded on Dextran coated iron oxide core nanoparticles. Dox-Dex-IO-NPs are more potent than free Doxorubicin and Dex-IO-NPs facilitate less drug use to kill cancer cells. Considering that the IC_{50} of free Doxorubicin for MCF-7 and MCF-7/1000nM Dox cells is in the range of 1.8 μM and 183 μM , the IC_{50} of Dox-Dex-IO-NPs is substantially low (nearly 2 and 7 times less than free Doxorubicin, respectively). This can be considered as a marked improvement on the efficiency of Doxorubicin. It should be emphasized that the loading of Doxorubicin on Dex-IO-NPs significantly overcomes Doxorubicin resistance on MCF-7/1000nM Dox cells. Due to the endosomal internalization of Doxorubicin loaded Dextran coated iron oxide core nanoparticles, Doxorubicin cannot be easily externalized by the efflux pumps.³⁶ Dox-Dex-IO-NPs significantly improved the efficacy of the anti-cancer drug, Doxorubicin.

Doxorubicin can both released from Dex-IO-NPs and diffused through nuclear pores. The efficacy of 10-15 nm Dex-IO-NPs was demonstrated as a Doxorubicin delivery vehicle, which is smaller than nuclear pores and enters across the cell and nuclear membrane.

Treatments of Dox-Dex-IO-NPs and free Doxorubicin have also changed the expression levels of regulators of the intrinsic apoptotic pathway. It has been shown that Survivin expression is a determinant of Doxorubicin response in breast cancer cells.⁹ According to our results, Survivin expression was up-regulated on untreated MCF-7/1000nM Dox cells. Since Survivin up-regulation could be regarded as the signature of Doxorubicin resistance, delivery of Doxorubicin by Dex-IO-NPs could prevent Survivin induction, which could be the potential mechanism for increased cytotoxicity of Dox-Dex-IO-NPs compared to free Doxorubicin.

We observed that the anti-apoptotic Bcl-2 gene was down-regulated in response to Dox-Dex-IO-NPs while upregulated by free Doxorubicin to prevent the apoptosis of MCF-7/1000nM Dox cells. So, Bcl-2 down-regulation could contribute to apoptosis of Dox-Dex-IO-NPs treated MCF-7/1000nM Dox cells. Whereas, expressions levels of pro-apoptotic Noxa, caspase 3 and p53 genes did not change significantly between the treated and untreated MCF-7/1000nM Dox cell lines ($p > 0,005$). Noxa, is upregulated in response to p53-mediated apoptosis. Noxa and p53 did not statistically upregulate in these cells ($p > 0,005$).

CONCLUSION

In this study, it was revealed that Doxorubicin resistance in MCF-7 breast cancer cells was bypassed by Dox-Dex-IO-NPs *in vitro*. We observed that the cellular internalization of Dox-Dex-IO-NPs was so high in Doxorubicin resistant MCF7 cells by fluorescence microscopy. Therefore, nanoparticles bypass the efflux mechanisms responsible for multidrug resistance. The cytotoxic efficacy of drug was increased nearly 7 folds when loaded on Dextran coated iron oxide core nanoparticles. Moreover, side effects of Doxorubicin on healthy tissues can be prevented by magnetic targeting of Dox-Dex-IO-NPs *in vivo* which will be in our future prospectives. Consequently, Dox-Dex-IO-NPs were far more efficient as an anti-cancer drug than free Doxorubicin, when releasing from Dex-IO-NPs through natural degradation of dextran, allowing free diffusion and accumulation of Doxorubicin in the nucleus to achieve the high apoptotic activity.

CONFLICT OF INTEREST: Authros declare no conflict of interest.

REFERENCES AND NOTES

1. A.A. Petryk, A.J. Giustini, R.E. Gottesman, P.A. Kaufman, P.J. Hoopes. Magnetic nanoparticle hyperthermia enhancement of cisplatin chemotherapy cancer treatment. *Int. J. Hyperth.* **2013**, 29 (8), 845–851.
2. C. Sun, J.S.H. Lee, M. Zhang. Magnetic nanoparticles in MR imaging and drug delivery. *Adv. Drug Deliv. Rev.* **2008**, 60 (11), 1252–1265.
3. J.S. Weinstein, C.G. Varallyay, E. Dosa, et al. Superparamagnetic iron oxide nanoparticles: Diagnostic magnetic resonance imaging and potential therapeutic applications in neurooncology and central nervous system inflammatory pathologies, a review. *J. Cereb. Blood Flow Metab.* **2010**, 30 (1), 15–35.

4. L. Gu, R.H. Fang, M.J. Sailor, J.H. Park. In vivo clearance and toxicity of monodisperse iron oxide nanocrystals. *ACS Nano* **2012**, 6 (6), 4947–4954.
5. C.G. Stirrat, D.E. Newby, J.M.J. Robson, M.A. Jansen. The Use of Superparamagnetic Iron Oxide Nanoparticles to Assess Cardiac Inflammation. *Curr. Cardiovasc. Imaging Rep.* **2014**, 7 (5), 1–8.
6. S. Martel. Presenting a new paradigm in cancer therapy: Delivering therapeutic agents using navigable microcarriers. *IEEE Pulse* **2014**, 5 (3), 48–55.
7. M. Mobahat, A. Narendran, K. Riabowol. Survivin as a preferential target for cancer therapy. *Int. J. Mol. Sci.* **2014**, 15 (2), 2494–2516.
8. R.C. Arend, A.I. Londoño-Joshi, J.M. Straughn, D.J. Buchsbaum. The Wnt/ β -catenin pathway in ovarian cancer: A review. *Gynecol. Oncol.* **2013**, 131 (3), 772–779.
9. A. Faversani, V. Vaira, G.P. Moro, et al. Survivin family proteins as novel molecular determinants of doxorubicin resistance in organotypic human breast tumors. *Breast Cancer Res.* **2014**, 16 (3).
10. P.E. Czabotar, G. Lessene, A. Strasser, J.M. Adams. Control of apoptosis by the BCL-2 protein family: Implications for physiology and therapy. *Nat. Rev. Mol. Cell Biol.* **2014**, 15 (1), 49–63.
11. A.G. Porter, R.U. Jänicke. Emerging roles of caspase-3 in apoptosis. *Cell Death Differ.* **1999**, 6 (2), 99–104.
12. G.M. Cohen. Caspases: The executioners of apoptosis. *Biochem. J.* **1997**, 326 (1), 1–16.
13. R.S. Akhtar, Y. Geng, B.J. Klocke, et al. BH3-only proapoptotic Bcl-2 family members Noxa and Puma mediate neural precursor cell death. *J. Neurosci.* **2006**, 26 (27), 7257–7264.
14. Levine AJ. P53, the Cellular Gatekeeper for Growth and Division. *Cell* **1997**, 88, 323.
15. P. Mittal, S. Singh, A. Singh, I.K. Singh. Current advances in drug delivery systems for treatment of Triple negative breast cancer (TNBC). *Chem. Biol. Lett.* **2020**, 7 (1), 1–12.
16. B.S. Chhikara, B. Rath, K. Parang. Critical evaluation of pharmaceutical rational design of Nano-Delivery systems for Doxorubicin in Cancer therapy. *J. Mater. Nanosci.* **2019**, 6 (2), 47–66.
17. B.S. Chhikara. Current trends in nanomedicine and nanobiotechnology research. *J. Mater. Nanosci.* **2017**, 4 (1), 19–24.
18. P. Pant, C. Gupta, S. Kumar, et al. Curcumin loaded Silica Nanoparticles and their therapeutic applications: A review. *J. Mater. Nanosci.* **2020**, 7 (1), 1–18.
19. S.S. Malapure, S. Bhushan, R. Kumar, S. Bharati. Radiolabelled nanoparticles in cancer management: current status and developments. *Chem. Biol. Lett.* **2018**, 5 (1), 25–34.
20. S.K. Sahu, S. Maiti, A. Pramanik, S.K. Ghosh, P. Pramanik. Controlling the thickness of polymeric shell on magnetic nanoparticles loaded with doxorubicin for targeted delivery and MRI contrast agent. *Carbohydr. Polym.* **2012**, 87 (4), 2593–2604.
21. X. He, X. Wu, X. Cai, et al. Functionalization of magnetic nanoparticles with dendritic-linear-brush-like triblock copolymers and their drug release properties. *Langmuir* **2012**, 28 (32), 11929–11938.
22. J. Gautier, E. Allard-Vannier, E. Munnier, M. Soucé, I. Chourpa. Recent advances in theranostic nanocarriers of doxorubicin based on iron oxide and gold nanoparticles. *J. Control. Release* **2013**, 169 (1–2), 48–61.
23. S. Yalcin, G. Unsoy, P. Mutlu, R. Khodadust, U. Gunduz. Polyhydroxybutyrate-coated magnetic nanoparticles for doxorubicin delivery: Cytotoxic effect against doxorubicin-resistant breast cancer cell line. *Am. J. Ther.* **2014**, 21 (6), 453–461.
24. K. Rouhollah, M. Pelin, Y. Serap, U. Gozde, G. Ufuk. Doxorubicin loading, release, and stability of polyamidoamine dendrimer-coated magnetic nanoparticles. *J. Pharm. Sci.* **2013**, 102 (6), 1825–1835.
25. G. Unsoy, R. Khodadust, S. Yalcin, P. Mutlu, U. Gunduz. Synthesis of Doxorubicin loaded magnetic chitosan nanoparticles for pH responsive targeted drug delivery. *Eur. J. Pharm. Sci.* **2014**, 62, 243–250.
26. I. Roy, A. Anuradha. Synthesis and characterization of iron phosphate NPs and applications in magnetically guided drug delivery. *J. Mater. Nanosci.* **2016**, 3 (1), 1–7.
27. F. Yang, S.S. Teves, C.J. Kemp, S. Henikoff. Doxorubicin, DNA torsion, and chromatin dynamics. *Biochim. Biophys. Acta - Rev. Cancer* **2014**, 1845 (1), 84–89.
28. H. Jang, S.R. Ryoo, K. Kostarelos, S.W. Han, D.H. Min. The effective nuclear delivery of doxorubicin from dextran-coated gold nanoparticles larger than nuclear pores. *Biomaterials* **2013**, 34 (13), 3503–3510.
29. P. Yousefpour, F. Atyabi, E.V. Farahani, R. Sakhtianchi, R. Dinarvand. Polyanionic carbohydrate doxorubicin-dextran nanocomplex as a delivery system for anticancer drugs: in vitro analysis and evaluations. *Int. J. Nanomedicine* **2011**, 6, 1487–1496.
30. C.E. Mora-Huertas, H. Fessi, A. Elaissari. Polymer-based nanocapsules for drug delivery. *Int. J. Pharm.* **2010**, 385 (1–2), 113–142.
31. J. Zhang, R.D.K. Misra. Magnetic drug-targeting carrier encapsulated with thermosensitive smart polymer: Core-shell nanoparticle carrier and drug release response. *Acta Biomater.* **2007**, 3 (6), 838–850.
32. O. Tacar, P. Sriamornsak, C.R. Dass. Doxorubicin: An update on anticancer molecular action, toxicity and novel drug delivery systems. *J. Pharm. Pharmacol.* **2013**, 65 (2), 157–170.
33. B.S. Chhikara, D. Mandal, K. Parang. Synthesis, anticancer activities, and cellular uptake studies of lipophilic derivatives of doxorubicin succinate. *J. Med. Chem.* **2012**, 55 (4), 1500–1510.
34. C.F. Thorn, C. Oshiro, S. Marsh, et al. Doxorubicin pathways: Pharmacodynamics and adverse effects. *Pharmacogenet. Genomics* **2011**, 21 (7), 440–446.
35. G. Xiong, Y. Chen, E.A. Arriaga. Measuring the doxorubicin content of single nuclei by micellar electrokinetic capillary chromatography with laser-induced fluorescence detection. *Anal. Chem.* **2005**, 77 (11), 3488–3493.
36. F.M. Kievit, F.Y. Wang, C. Fang, et al. Doxorubicin loaded iron oxide nanoparticles overcome multidrug resistance in cancer in vitro. *J. Control. Release* **2011**, 152 (1), 76–83.